PHYSICAL REVIEW B, VOLUME 64, 075416

Microstructure and residual strain in La_2CuO_4 thin films on $LaSrAlO_4$-buffered $SrTiO_3$ substrates

C. L. Jia,[1] X. H. Zeng,[2] X. X. Xi,[2] and K. Urban[1]
[1]*Institut für Festkörperforschung, Forschungszentrum Jülich GmbH, D-52425 Jülich, Germany*
[2]*Department of Physics, Pennsylvania State University, University Park, Pennsylvania 16802*
(Received 31 January 2001; published 27 July 2001)

The microstructure and residual strain of bilayer films of $La_2CuO_4/LaSrAlO_4$ on $SrTiO_3$ substrates are investigated by means of electron-diffraction analysis and high-resolution transmission electron microscopy. In two samples containing $LaSrAlO_4$ buffer layers with thicknesses of 37 and 75 nm, a compressive strain is measured in the La_2CuO_4 layers. From the presence of lattice defects close to interface imperfections it can be concluded that the thickness of these La_2CuO_4 layers is close to the critical value for mismatch-strain relaxation. The strain level in the layer on the 37-nm-thick buffer is lower than that in the layer on the 75-nm buffer. A high density of planar shear defects is observed which can be introduced by steps of the substrate surface and by stacking faults in the film. Interfacial stacking faults are found at the interface between the La_2CuO_4 and the $LaSrAlO_4$ layers. Interface roughening can hinder the formation of these faults. In addition, a strong roughness of the interface is found to induce strong lattice bending and extra strain in the La_2CuO_4 layer.

DOI: 10.1103/PhysRevB.64.075416 PACS number(s): 68.35.−p, 68.37.Lp, 74.76.−w

I. INTRODUCTION

Recently considerable research efforts have been directed towards the production and optimization of thin films of electroceramic oxide materials due to their large potential for application in modern electronic devices.[1] Depending on the substrates and the preparation conditions employed, the microstructure of the films can be considerably different from that found in bulk materials with respect to the configuration of lattice defects and strain state. These structural features lead to a deviation of the electrical properties compared to those in the bulk. A compressive epitaxial strain in thin films of $La_{2-x}Sr_xCuO_4$ has been found to increase its superconducting transition temperature.[2] The strain is mainly due to the lattice mismatch between film and substrate. The actual strain level depends on the film thickness. When the film thickness exceeds a critical value the misfit strain is relaxed by the introduction of misfit dislocations at the interface between film and substrate. In many cases, strain is also induced by a difference in the thermal-expansion coefficients between film and substrate. The strain level in the films can be also controlled by employing suitable buffer layers between substrate and film. For instance, the superconducting properties of La_2CuO_4 thin films were found to depend on the layer thickness of a $LaSrAlO_4$ buffer in the $La_2CuO_4/LaSrAlO_4/SrTiO_3$ system.[3]

At room temperature La_2CuO_4 (in the following abbreviated as LCO) exhibits an orthorhombic structure with lattice parameters $a_0=0.533\,46$ nm, $b_0=0.541\,48$ nm, and $c_0=1.311\,72$ nm. $LaSrAlO_4$ (abbreviated as LSAO) has a tetragonal structure with lattice parameters $a=0.3754$ nm and $c=1.2635$ nm. $SrTiO_3$ (abbreviated as STO) shows a typical cubic perovskite structure with a lattice parameter $a=0.3905$ nm. The structure of La_2CuO_4 is very similar to that of $LaSrAlO_4$. The difference is in the small orthorhombic distortion (about 0.5%) of the La_2CuO_4 lattice. For convenience in comparison with $LaSrAlO_4$ and $SrTiO_3$, in the following discussion we neglect the small orthorhombic distortion of the La_2CuO_4 lattice and regard it as pseudotetragonal with lattice parameters $a=(a_0^2+b_0^2)^{1/2}/2=0.380\,05$ nm and $c=c_0=1.311\,72$ nm. Figure 1 shows the unit cells of the three compounds. In the film system of $La_2CuO_4/LaSrAlO_4/SrTiO_3$, we have, according to the above lattice parameters, the nominal lattice mismatch $(a_{LCO}-a_{LSAO})/a_{LCO}=0.01224$ for $La_2CuO_4/LaSrAlO_4$ and $(a_{LSAO}-a_{STO})/a_{LSAO}=-0.040\,22$ for $LaSrAlO_4/SrTiO_3$. The mismatch with positive sign can induce a compressive stress in the film while that with negative sign produces a tensile stress.

In the present work we report on a study by means of conventional transmission electron microscopy (TEM) and high-resolution transmission electron microscopy (HRTEM) on the microstructure and remaining strain in the LCO films grown on the LSAO buffer layers with different thickness on $SrTiO_3$ substrates. Our investigations are focused on the possible effects of the thickness of LSAO buffer layers, the mi-

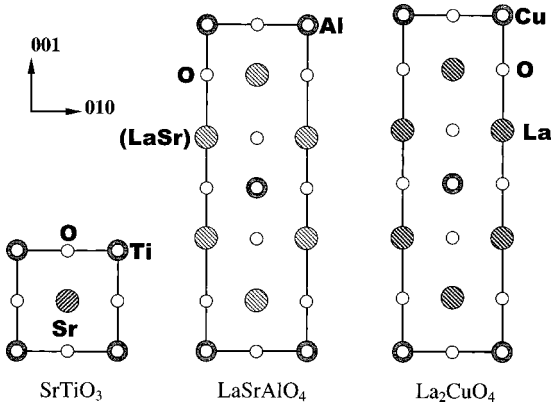

FIG. 1. [100] projection of unit cells of $SrTiO_3$, $LaSrAlO_4$, and La_2CuO_4.

crostructure, and the defects on the strain level and distribution.

II. EXPERIMENTAL DETAILS

Two types of LCO samples, referred to as *A* and *B*, were prepared for the TEM investigations by pulsed-laser deposition (PLD) on LSAO-buffered (001) STO substrates. The buffer-layer thickness was chosen as 40 nm for sample *A* and 80 nm for sample *B*. The thickness of the LCO layer in both samples was 20 to 26 nm. This thickness is considered to be below the critical value for the occurrence of significant misfit strain relaxation by the introduction of interface defects. The LSAO buffer layer was deposited at a substrate temperature of 780 °C and the LCO layer at 700 °C in an atmosphere of pure molecular oxygen with a pressure of 100 mTorr. Then the samples were cooled down to room temperature in pure molecular oxygen at a pressure of 760 Torr. Details of the PLD conditions are discussed in Ref. 4.

Cross-sectional samples were prepared for TEM and HRTEM investigations. Slices of $2\times1\ \mathrm{mm}^2$ in size were cut from the film-covered wafers along the (100) plane of the STO substrate. Two of the slices were glued face to face and then embedded in epoxy resin. After the glue had been cured disks of 3 mm in diameter were obtained by cutting away redundant epoxy. These disks were then mechanically ground, dimpled, and polished from both sides until the thickness of the central area was less than 10 μm. The final thinning was performed by means of ion milling on a sample stage cooled by liquid nitrogen. The TEM and HRTEM investigations were carried out on a JEOL 4000EX electron microscope operated at 400 kV. Image simulations were carried out using the EMS computer program[5] in order to clarify the experimental results. The parameters used for image simulation were 1 mm for the spherical aberration coefficient, 12 nm for the defocus spread, 1 mrad for the semiconvergence angle of illumination, and 11 nm^{-1} for the diameter of the objective lens aperture.

III. RESULTS

A. General morphology and lattice parameters of the films

TEM investigations showed that the microstructure of both samples *A* and *B* looks very similar. Fully expitaxial relations are maintained by the LCO layer and the LSAO buffer layer of the two samples with their *c* axes parallel to the substrate normal, the [001] direction of STO. With respect to the tetragonal description for the LCO compound, we obtained the orientation relationships

$$(001)_{\mathrm{LCO}}\|(001)_{\mathrm{LSAO}}\|(001)_{\mathrm{STO}},$$

$$[100]_{\mathrm{LCO}}\|[100]_{\mathrm{LSAO}}\|[100]_{\mathrm{STO}},$$

and

$$[010]_{\mathrm{LCO}}\|[010]_{\mathrm{LSAO}}\|[010]_{\mathrm{STO}}$$

between the film layers and the substrate.

Figure 2 shows a cross-sectional overview of sample *A*. The clearly visible lattice fringes in the film layers indicate the typical feature of a *c*-axis-oriented film. The interfaces between the film and the substrate and between the LCO layer and the LSAO buffer layer look sharp as marked by two horizontal arrows. Nevertheless, the contrast of the upper interface appears to be better developed compared to that of the lower one, indicating a lower defect density and less distortion in the nearby lattice. A high density of dark diffuse linelike contrasts can be seen starting from the interface between the buffer layer and the substrate and penetrating in most cases the full thickness of the buffer layer. This line contrast originates from planar defects such as antiphase boundaries and shear defects.[6] In some cases, the defects extend across the LSAO/LCO interface into the LCO layer, as indicated by an open arrow. From the lattice fringe image the thickness of the LSAO layer and the LCO layer is measured as about 37 nm and about 20 nm, respectively, in agreement with the expected values.

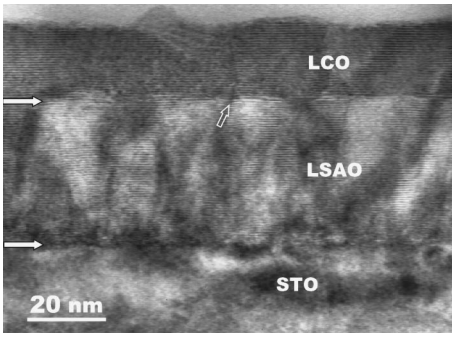

FIG. 2. Cross-sectional image of the bilayer film of LCO/LSAO on STO substrate. Two horizontal arrows mark the interfaces and a vertical arrow denotes a planar defect running across the interface into the LCO layer.

For sample *B*, we obtained similar results on the microstructure morphology except for the layer thickness and the interface morphology. In the *B*-type sample the interface between the LSAO buffer layer and the LCO layer looks wavy, showing a greater roughness than that in sample *A*. According to the measurements of the lattice image the LSAO buffer layer is 75 nm thick and the LCO layer is 22 nm thick in sample *B*.

The lattice parameters of the LCO and LSAO layer were determined from selected area electron-diffraction patterns (EPD's). The EPD's used are the superposed EPD's including the crystallographic information of both the film and the substrate recorded using a selected area aperture covering the whole thickness of the film and part of the substrate. Figure 3 shows such a superposed [100] zone-axis EPD of sample *A*. From the pattern the difference in the *c* axis between the three compounds can be clearly seen with the separation of their $\{00l\}$ reflection spots. The relaxation of the misfit strain in the LSAO layer is also visible from the separation of the reflection (040) from that of STO. The relaxation in the LCO layer with respect to the LSAO layer can only be recognized by checking the high index reflection spots, as marked by the white lines. Qualitatively, in the two samples both the epitaxial layers show more or less strain relaxation.

In the calculation of the lattice parameters of the films we referred to the reflections and the bulk parameter of STO as

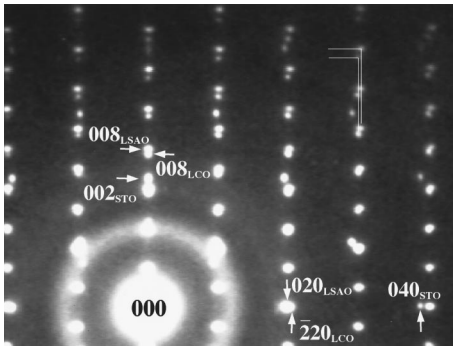

FIG. 3. A superposed electron-diffraction pattern from sample *A* including three [100] zone axis patterns of the LCO layer, the LSAO layer, and the STO substrate. The orthogonal lines show the separation of the reflection spots of the LCO layer from those of the LSAO layer.

the calibration standard in the superposed EPD's. The determination of the lattice parameters of the different film layers was carried out as follows. Firstly, the EPD's were digitized and the centers of the reflection spots were determined using a center-of-mass approach and coordinated by means of the DigitalMicrograph software package. The spots with high indexes were chosen in the calculation since they are well separated from each other for LCO, LSAO, and STO, leading to a more reliable determination of the mass centers. Secondly, the period distances along the [010]* and [001]* reciprocal directions, corresponding to (010) and (001) plane spacings, were calculated according to the coordinates of the respective reflection spots. The calculated distances were averaged in the two directions to obtain mean values for the two type distances. These mean distances were used to calculate the lattice parameters of the LSAO and LCO layers in comparison with the standard (010) and (001) spacing of STO. The calculated results are listed in Table I. In comparison with the *a*-axis parameter of the bulk, the LCO layers in both samples *A* and *B* are under compressive strain. The level of the compressive strain of the LCO layer in sample *A* is lower than that in sample *B*. The layer of LSAO is under tensile strain in sample *A*. The misfit strain in the LSAO layer in sample *B* is almost fully relaxed according to the calculated parameters.

B. Lattice defects and local strain

As indicated by Fig. 2, the films contain many defects. In the layers of LSAO and LCO, due to the similarity of the crystal structure, we find a similar structural behavior of the lattice defects. These defects are, in most cases, formed at the interface between film and substrate, induced by steps on the substrate surface. The density of the defects is higher in the LSAO buffer layer than in the LCO layer. Figure 4 shows a [100] lattice image of the interface area between the LSAO buffer layer and the substrate. The arrow marks an interface step. Directly above this step, a planar shear defect occurs and divides the film into two parts with a relative shift of a fraction of a unit cell as marked by rectangles. Similar defects were reported by Alimoussa *et al.*[6] We found that the displacement vector of the defects in the film can be different, depending on the step height. At this step we also find a misfit dislocation with a Burgers vector $a[010]$.

TABLE I. Lattice parameters of the LCO and the LSAO layers on STO substrates calculated from superposed electron diffraction patterns with reference to the reflection spots of STO. In sample *A* the thickness of the LCO and the LSAO layer is 20 and 37 nm, respectively. In sample *B* the thickness values for the two layers are 22 and 75 nm, respectively.

Axis	a_{LCO} (nm)	c_{LCO} (nm)	a_{LSAO} (nm)	c_{LSAO} (nm)
Bulk	0.38005	1.31172	0.3754	1.2635
Sample *A*	0.3788	1.3191	0.3756	1.2706
Sample *B*	0.3780	1.3204	0.3754	1.2716

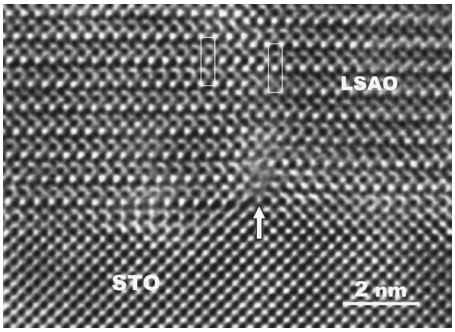

FIG. 4. [100] lattice image of the interface between the LSAO buffer layer and the STO substrate. An arrow shows an interfacial step which introduces a planar shear defect into the film. A misfit dislocation is located right above the step.

Figure 5 shows a lattice image of a (001) stacking fault inducing two shear defects marked by arrows in the LSAO buffer layer. By means of image simulation, the AlO_2 plane was identified and is denoted by white lines in this image. The stacking fault occurs clearly with the insertion of an extra plane of (LaSr)O between a (LaSr)O plane and an AlO_2 plane, forming a structure feature of triple (LaSr)O planes stacking along the [001] direction. The shift in the (001) plane and the spacing between (LaSr)O planes in the structure (Fig. 1) is $\frac{1}{2}[110]$ and close to $\frac{1}{6}[001]$, respectively. The displacement vector of the shear defects must correspondingly be $\frac{1}{6}[331]$ since no other defects occur in this area. This type of defect can stop in the lattice leaving a dislocation with a Burgers vector having the same value as the displacement vector of the shear defect. Figure 6 displays an image

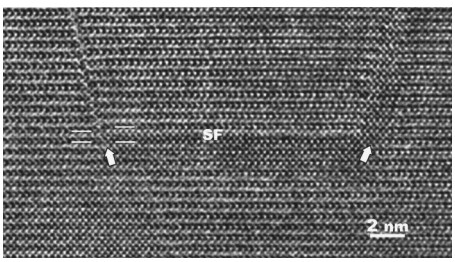

FIG. 5. [100] image of the LSAO buffer layer demonstrating a (001) stacking fault. Two shear defects denoted by arrows are formed at the two ends of the fault. The white lines mark the AlO_2 planes.

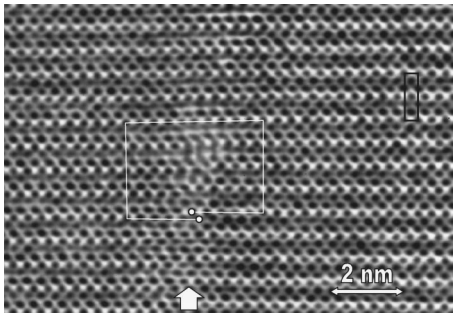

FIG. 6. [100] image showing that a shear defect (arrow) stops in the film and leaves a dislocation.

showing such a configuration. A vertical arrow indicates a shear defect with the same structural feature as those in Fig. 5. This defect disappears in the middle area where a dislocation can be recognized. A Burgers circuit surrounding the dislocation leads to a Burgers vector $(a/6)[031]$. Since the component of the Burgers vector along the [100] viewing direction is not visible, the vector $(a/6)[031]$ can also be a component of the Burgers vector $(a/6)[331]$.

In the LCO layer, the shear defects are found to occur either as a continuity of the defects in the LSAO layer across the interface, or originating from the formation of a stacking fault at the interface. The stacking fault occurring at the interface is different from that within the LSAO layer shown in Fig. 5. Figure 7(a) shows a lattice image of an interface between the LSAO and the LCO layers with an interfacial stacking fault. The interface can be localized by checking the *c*-axis parameter of the two compounds across the interface area since the *c*-axis parameter of LCO is larger than that of LSAO as marked by two rectangles. The stacking atomic planes along the *c* axis were identified by means of image simulations. In Fig. 7(a) the black arrows denote the AlO_2 plane in the LSAO layer and the white arrows the CuO_2 plane in the LCO layer. At the interface the gray arrows mark the plane of either AlO_2 or CuO_2. Due to the small difference

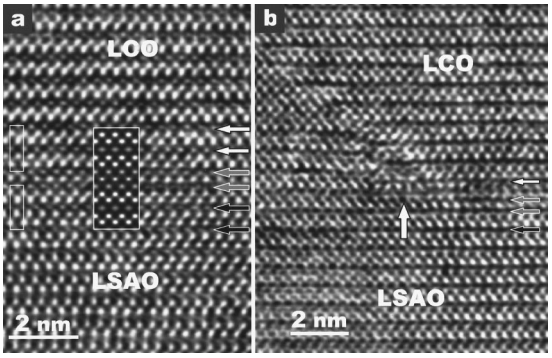

FIG. 7. (a) [100] image of an interfacial stacking fault marked by two gray arrows at the interface between the LCO and the LSAO layers. The black and the white arrows show the AlO_2 and the CuO_2 planes, respectively. The inset shows a simulated image of the stacking fault calculated for a sample thickness of 5.5 nm and a defocus value of −10 nm. The dashed line frame and the solid line denote the unit cells of LSAO and LCO, respectively. (b) A shear defect starting from an end of the interfacial stacking fault.

in image contrast of the two planes it is very difficult to distinguish them from each other. Therefore we denote the two planes as MO_2 (*M* for Al or Cu). Nevertheless, it is easily recognizable that the spacing between two adjacent MO_2 planes is smaller than that between two AlO_2 planes or that between two CuO_2 planes in the layer matrixes. A structure model of the interface stacking fault was arranged according to the above analysis. The best fit between the simulated image and the experimental image was obtained for a sample thickness of 5.5 nm and a defocus value of −10 nm. The simulated image is inserted in Fig. 7(a). There is one LaO or (LaSr)O plane only between the two MO_2 planes, while a double plane of LaO exists between two CuO_2 planes in the normal structure (Fig. 1). Similar defects were also observed in a Sr-doped LCO film on a LSAO substrate.[7] This type of interfacial stacking fault was frequently observed in sample A. However, it was rarely found at the interface in sample *B*, which exhibits a larger roughness than that in sample *A*. Since the two samples were prepared under the same conditions the different level of roughness can be considered as a factor for controlling the formation of the interfacial stacking faults. At the end of this type defect a shear planar defect is usually introduced running into the LCO layer. Figure 7(b) shows a lattice image of an interfacial stacking fault end. A shear defect starts at the end. In addition, we can also find a dislocation, as denoted by a vertical arrow, by looking at the image at a glancing angle along the diagonal directions.

Due to the existence of the lattice defects and secondary phase precipitates, which were also observed in the films, the areas including these defects lattice distortions were observed. Therefore, the strain distribution in the LCO layer must be inhomogeneous due to the existence of these defects. The strain state can be also changed by the different morphology of the interface. Figure 8(a) shows a [100] lattice image of an interface area not disturbed by lattice defects. The interface between the LSAO buffer layer and the LCO layer looks perfect. Under the imaging conditions applied the contrast difference between the two layers is not sufficient to be used in localizing the interface. The interface can be determined only by checking the difference in the *c*-axis parameter of the two compounds as marked by a dashed line. In the left part of Fig. 8(a) two dashed line frames denote the dimension of two LSAO unit cells stacking along the *c* axis and a solid-line frame marks two unit cells of LCO. The difference in the *c*-axis parameter is clearly seen by comparing the two type frames. In this area the strain in the LCO layer and in the LSAO layer can be considered as homogeneously distributed in the film plane. In contrast, Fig. 8(b) shows a rough interface area with lattice defects. A curved dashed line marks the interface between the LASO and the LCO layers. An arrow at the top of the interface hill points out a dislocation with a Burgers vector $a[010]$. The interface was firstly determined according to image contrast change, which can be more easily recognized under a low magnification. The LCO layer exhibits a little darker contrast than the LSAO layer. Secondly, the determination was further verified by checking the *c*-lattice parameters. Similar to Fig. 8(a), the dashed line frames show two

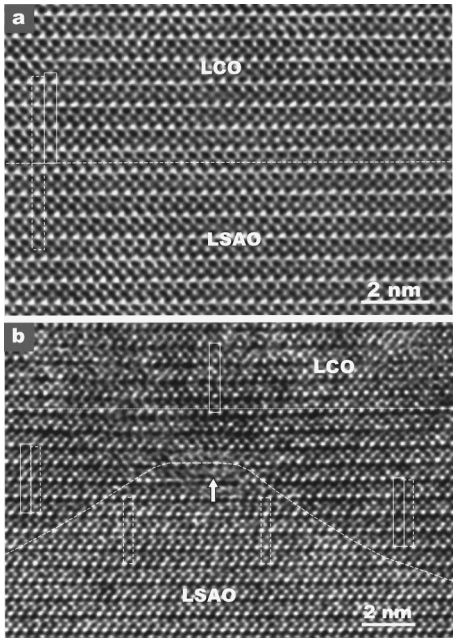

FIG. 8. [100] images of (a) a flat and perfect interface and (b) a rough interface between the LCO layer and the LSAO layer. The dashed lines trace the interface and the dotted line shows the bending of the lattice plane. An arrow shows a dislocation at the top of interface hillock. The dashed line frames and the solid line frames denote the dimension of two unit cells of LSAO and LCO stacking in the *c*-axis direction, respectively.

unit cells of LSAO and the solid-line frame show two unit cells of LCO. The *c*-lattice fringes of the LSAO layer in the lower part of the image look clear and straight, indicating a relatively perfect nature of the lattice. In the LCO layer, the upper part of Fig. 8(b), one can recognize an irregularity of the image contrast which is indicative of a local change of the strain level and lattice distortion. A strong bending of the *c* planes of the LCO layer is evidently due to the interface hill and the dislocation. The bending can be easily recognized by comparing the *c*-plane fringes with the straight dotted line.

IV. DISCUSSION

Based on electron-diffraction patterns, our results show different *a*-lattice parameters for the LCO layer on the LSAO buffers with a different thickness on a subangstrom scale. On an absolute scale, due to the limited accuracy of the electron-diffraction pattern, the obtained lattice parameter values are not very precise. In our case, however, the relative lattice parameter values are easily obtained with high precision by electron diffraction. For this we employ a reference to the STO diffraction pattern contributing to the same EPD's of the film systems. Therefore, the main deviation is the measurement errors which are within 0.15%. On the other hand, the digitized patterns and the large number of reflection spots used can also improve the accuracy of the measurement in comparison to a manual measurement directly from a diffraction pattern. Indeed, the results agree quite well with those obtained from x-ray measurements.[3] In comparison to the lattice parameters of bulk materials the LCO layer in the films suffers from compressive strain with different levels relating to the thickness of the buffer layers. An in-plane compressive strain level of 0.33% and 0.54% is obtained in a 20-nm LCO layer on a 37-nm-thick buffer layer and in a 22-nm layer on a 75-nm-thick buffer of LSAO, respectively. This amount of compressive strain is sufficient to change the properties of the LCO compound.[3]

At the interface between the LSAO layer and the STO substrate we observed regularly distributed misfit dislocations. This means that the thickness of the buffer in both samples exceeds the critical thickness in the LSAO/STO system. The thicknesses of 20 nm in sample *A* and 22 nm in sample *B* should be close to the critical value for the LCO layer in the LSAO/LCO system, since dislocations with Burgers vectors for relaxation of the lattice misfit were found at the interface. This is indicative of the existence of misfit strain relaxation. On the other hand, we note that the dislocations are not isolated but usually related to other defects. The local strain due to defects can locally increase the driving force for misfit dislocation formation and enhance the nucleation of the dislocation even if the thickness of the film does not yet fully reach the critical value.

The different levels of the strain in the LCO layer of the two samples can be considered to be a result of the effects coming from both the LCO layer and the LSAO layer. Due to the low value of the thickness of the LSAO layer in sample *A*, in addition to the straining from the substrate, the geometrical constraints originating from the LCO layer must also be taken into account. In comparison with the thickness (20 nm) of the LCO layer the 37-nm thickness of the LSAO buffer layer, which is sandwiched between the LCO layer and the STO substrate, is not sufficient to entirely screen the straining effect originating from the misfit of the LCO layer, leading to an extra tensile strain in the LSAO layer. In this case, the low strain level of the LCO layer in sample *A* is partially based on expanding the buffer layer. In the film system of sample *B*, the buffer layer (75 nm) is much thicker than the LCO layer (22 nm). The straining effect from both the substrate and the LCO layer should be much smaller than the case of sample *A*. A higher level of strain is expected in the LCO layer than in sample *A*.

Besides the general strain in the LCO layer, we found a local strain variation on a microscale. The high density of lattice defects is one of the factors responsible for this. The other important factor is the morphology of the interface. In sample *B*, the interface between the buffer layer and the LCO layer has greater roughness than that in sample *A*. The lattice images reveal the effect of the roughness on the local strain in the LCO layer. Due to the large difference in *c*-lattice parameters between LSAO (1.2635 nm) and LCO (1.311 72 nm), across a surface hill of the buffer layer a strong bending is introduced into the lattice of the LCO layer. This strong bending produces an extra compressive stress in that part of the LCO layer directly above the hill tip and an extra tensile stress in the LSAO layer directly below the tip. These extra opposite stresses across the interface hill are equivalent to increasing the lattice mismatch locally. The value of critical thickness for mismatch relaxation decreases with the value of

the lattice mismatch of a system. The dislocations can be easily introduced in the area with extra stress even if the LCO layer does not exceed the critical thickness. From the lattice image of Fig. 8(b), the dislocation is likely introduced in this way. This dislocation located at the interface hill does not only relax the extra stress locally but also enhance the lattice bending. The strain relating to the lattice bend still remains in the layer. In a thin layer of LCO with such a wavy interface to a LSAO layer the strain level is expected to oscillate across the tip and valley of the interface hills with respect to the value of general strain measured from the diffraction pattern. In order to understand the details of the property behavior of the LCO layer, the local change of the strain level should also be taken into account.

An important difference in the lattice defect configuration between the two samples is the existence of the interfacial stacking faults in sample *A*. The formation of the interfacial stacking faults can be related to the relatively flat interface in this sample. The interfacial stacking faults were found in most cases to have a structure of a cubiclike unit which is smaller than one-third of the *c* parameters of the LCO and LSAO compounds. On a rough surface containing a high density of steps, which are usually a full *c* parameter in height, the formation of the stacking faults can induce a high density of shear defects or antiphase boundaries. This situation would dramatically increase the system energy. Therefore, interfacial stacking faults at a rough interface are energetically unfavorable. In contrast, the appearance of the faults on a flat surface does not cause such problems. If the energy of the faults is relatively low it cannot be avoided at the interface due to the possible fluctuation in the stoichiometry of coming materials induced by changing the targets.

V. CONCLUSION

The microstructure and strain state of epitaxial bilayer films of LCO/LSAO on the STO substrate are investigated by conventional and high-resolution transmission electron microscopy. Measurements on the digitized diffraction patterns permits us to determine the different levels of compressive strain remaining in the LCO layers on the LSAO buffer layers with different thicknesses. For a 37-nm-thick LSAO buffer layer a compressive strain of 0.33% is measured in a 20-nm-thick LCO layer, while on a buffer layer with a thickness of 75 nm a LCO layer with a thickness of 22 nm contains 0.54% compressive strain. A high density of planar shear defects has been observed which can be induced by steps on the substrate and by stacking faults in the film. Interfacial stacking faults are found to appear at the relatively flat interface between the LCO layer and the LSAO layer. Roughening of the interface is believed to have an obstructing effect on the formation of the interfacial stacking faults. Both the lattice defects and the interface roughening can induce a variation of local strain level. The effect of the interface roughness acts by the large lattice mismatch along the *c*-axis direction between LCO and LSAO.

ACKNOWLEDGMENTS

The authors are grateful to Dr. K. Tillmann for fruitful discussions. The work at Penn State is supported in part by NSF under Grant No. 9623889 and ONR under Grant No. N00014-00-1-0294.

[1] N. Setter and R. Waser, Acta Mater. **48**, 151 (2000).
[2] J.-P. Locquet, J. Perret, J. Fompeyrine, E. Mächler, J. W. Seo, and G. Van Tendeloo, Nature (London) **394**, 453 (1998).
[3] Weidong Si and X. X. Xi, Appl. Phys. Lett. **78**, 240 (2001).
[4] W. Si, H.-C. Li and X. X. Xi, Appl. Phys. Lett. **74**, 2839 (1999).
[5] P. Stadelmann, Ultramicroscopy **21**, 131 (1987).
[6] A. Alimoussa, M.-J. Casanove, and J. L. Hutchison, Philos. Mag. A **76**, 907 (1997).
[7] J. W. Seo, J. Perret, J. Fompeyrine, G. Van Tendeloo, and J.-P. Locquet, Proc. SPIE **3418**, 300 (1998).